

Overview of the Latest Scientific Results of China's Lunar Exploration Program

CHEN Yuesong¹ HAN Juanjuan¹ FAN Yu¹

ZOU Yongliao^{1,2} WANG Chi^{1,2}

¹(National Space Science Center, Chinese Academy of Sciences, Beijing 100190)

²(State Key Laboratory of Space Weather, National Space Science Center, Chinese Academy of Sciences, Beijing 100190)

Abstract China's Chang'E-4 probe successfully landed on 3 January 2019 in Von Kármán crater within the South Pole-Aitken (SPA) basin on the lunar far side. Based on the data acquired by the scientific payloads onboard the lander and the rover, the researchers obtained the related information such as the geologic and tectonic setting of the landing area, compositional characteristics of the landing surface materials, dielectric permittivity and density of the lunar soil. The experiments confirmed the existence of materials dominated by olivine and low-calcium pyroxene in the SPA basin on the lunar far side, which preliminary revealed the geological evolution history of the SPA basin and even that of the early time lunar crust, as well as the tectonic setting and formation mechanism of the materials in the lunar interior. The researchers also investigated the particle radiation, Linear Energy Transaction (LET) spectrum, and so forth on the lunar surface. The low-frequency radio observations were carried out on the lunar far side for the first time as well. This article summarizes the latest scientific results in the past years, focusing on the Chang'E-4 mission.

Key words CLEP, Chang'E-4, Scientific objectives, Scientific payloads, Scientific results

Classified index V 475

1 Overview of China's Lunar Exploration Program

China's Lunar Exploration Program (CLEP) has been divided into three main operational phases: lunar orbiting, soft-landing, and sample return. Lunar orbiting means remote sensing exploration around the Moon, which was successfully implemented by Chang'E-1 mission in October 2007 (http://www.gov.cn/jrzg/2007-10/24/content_785388.htm). The global and comprehensive observations were carried out including the topographic and geomorphologic characteristics of the lunar, material compositions of the lunar surface, the characteristics of the lunar soil and the Earth-Moon space environment.

After the successful implementation of Chang'E-1 mission, as the backup spacecraft of Chang'E-1 and the precursor mission of the soft-landing phase of CLEP, Chang'E-2 underwent an adaptive transformation, with the mandate to collect remote sensing data with higher precision and to image the candidate landing site of Chang'E-3. Chang'E-2 launched successfully in October 2010 and acquired the global lunar map with a resolution of 7 m. It flew by and explored the asteroid 4179 Toutatis in December 2012 (http://www.gov.cn/jrzg/2012-12/15/content_2290992.htm).

The second phase of CLEP refers to soft-landing and roving exploration on the lunar surface. As one of the missions scheduled in this phase, Chang'E-3

* Supported by National Key R&D Program of China (2020YFE0202100) and Beijing Municipal Science and Technology Commission (Z181100002918003)
Received September 11, 2020
E-mail: chen yuesong@nssc.ac.cn. Correspondence author: zouyongliao@nssc.ac.cn

was successfully launched in December 2013 (http://www.gov.cn/jrzg/2013-12/14/content_2547901.htm). As of now, it has carried out the activities to explore topography, geomorphology, tectonic geomorphology and sub-surface geotectonic of the Moon and to conduct research on the Earth's plasmasphere and astronomy by use of the Moon-based observation.

Chang'E-4 spacecraft was initially built as the backup of Chang'E-3. After the successful implementation of Chang'E-3, according to the worldwide development route of lunar exploration and China's overall thinking on future scientific researches on the Moon, the expert group made a very careful evaluation of Chang'E-4 mission based on the techniques of Chang'E-3 and finally selected the SPA Basin of the lunar far side as the landing and roving area, which gave Chang'E-4 a new scientific value.

After the relay communication satellite and Chang'E-4 probe were launched respectively in May 2018 and December 2018, Chang'E-4 probe made a successful landing on 3 January 2019 in the Von Kármán crater within the SPA basin on the Moon far side (177.6° east longitude and 45.5° south latitude), realizing the first soft-landing on the Moon's far side and the first relay communication between the lunar far side and the Earth in the human history (http://www.gov.cn/xinwen/2019-01/03/content_5354498.htm).

On 3 January 2020 (Beijing Time), Chang'E-4 completed work on its 13th lunar day and the rover traveled a total of 357.695 m. More than 210 GB of scientific data at all levels has been released publicly (<http://www.clep.org.cn/n5982341/c6808601/content.html>). A large number of scientific results has been published by China's Lunar Exploration Program^[1]. The paper mainly focuses on the latest major scientific results achieved by Chang'E-4 mission.

2 Scientific Objectives and Payloads of Chang'E-4

2.1 Scientific Objectives of Chang'E-4

The Chang'E-4 mission consists of three platforms: lander, rover and relay satellite. Four scientific goals were chosen in the Moon science, the lunar

space environment and low-frequency radio astronomy: (i) low-frequency radio astronomical study on the lunar surface; (ii) shallow structure investigation of the roving area on the lunar far side; (iii) the topographic and the mineralogical composition investigation of the roving area on the lunar far side; (iv) neutron radiation dose and neutral atom study on the lunar environment.

The chosen landing site for Chang'E-4 is the South Pole-Aitken Basin, which has been revealed to be a basin 2500 km in diameter with an average depth of more than 13 km, and recognized as the largest, oldest and deepest impact crater yet discovered in the solar system. It faithfully records the primary differentiation of the Moon, is a hot spot of lunar science^[2-4].

The SPA basin is thought to be formed from an impact that penetrated through the Moon's distinctive plagioclase rich crust, exposing the lunar lower crust and probably upper mantle material^[5-7]. It also contains some of the relatively few far side maria. Therefore, exploration of this region may address some fundamental questions, such as the nature of the lunar mantle, the cause of the greater crustal thickness on the far side, and how far side maria differ from their nearside counterparts. Furthermore, better constraints of the age of this basin may inform our understanding of the early impact flux on the Moon, and therefore also on the Earth^[6].

The SPA basin has been studied with spectral observations and recently been subdivided into four distinct compositional zones based on Moon Mineralogy Mapper (M3) data: (i) a central about 700-km-wide SPA Compositional Anomaly (SPACA), which exhibits a strong Ca-pyroxene signature, which is different from typical mare basalts; (ii) an Mg-Pyroxene Annulus, which is characterized by Mg-rich pyroxenes; (iii) a Heterogeneous Annulus, which exhibits mixing of localized pyroxene-rich units and feldspathic materials; and (iv) the SPA Exterior, which is mafic-free and dominated by feldspathic materials^[7]. The Chang'E-4 landing site is located at the eastern edge of the mare-containing Von Kármán crater, within the ejecta field of the nearby Finsen crater^[6]. The Von Kármán crater

(diameter $D = 186$ km; central coordinates as 44.4°S , 176.2°E) lies within the Mg-Pyroxene Annulus, just northwest of the SPACA terrain. Finsen crater (diameter $D = 73$ km; central coordinates as 42.3°S , 182.3°E)^[7]. This location was selected to optimize the likelihood of being able to investigate the crustal stratigraphy and regolith development, and to access material from farside maria, the deep crust, and possibly the mantle^[6].

Chang'E-4 lander and Yutu-2 rover carried a landing camera, a terrain camera, two panoramic cameras, an infrared imaging spectrometer, and a lunar penetrating radar^[2, 6]. These instruments enable an analysis of the topography, regolith, shallow structure, and rock and mineral compositions of the landing and roving sites^[6]. In situ exploration within the Von Kármán landing region brings unprecedented imaging, spectral, radar, and low-frequency radio spectral data for the landing region, and it greatly improves our understanding about the compositions of farside mare basalt, SPA compositional zones including SPA compositional anomaly and Mg-pyroxene annulus, regolith evolution, and the lunar space environment^[7].

Low-frequency radio astronomy in the frequency band below about 10 MHz cannot be done on the ground or be well done from space due to the Earth's ionosphere cut-off, man-made Radio Frequency Interference (RFI), and the Auroral Kilometric Radiation (AKR) noise^[2]. The lunar farside is shielded from radio interference from the Earth, blocks the RFI, the AKR noise from the Earth, as well as from solar emissions during the lunar night, so it is expected to be an excellent location for low-frequency radio astronomy^[2, 6]. The experiment uses the Low-frequency Radio Spectrometer on the lander, and the Netherlands-China Low-frequency Explorer on the relay satellite, to do joint low frequency radio astronomical observation. Its specific exploration goals include, to obtain the map of radio sky at 2 frequencies in the band of 1~80 MHz, to investigate the AKR in the band of 0.1~1 MHz, to observe the Jovian radio emission in the band of 1~40 MHz, to observe and study the disastrous space weather events and the Type II and III solar burst in the band

above 0.1 MHz^[2].

Based on the lunar surface platform, the researchers conducted the measurement of the comprehensive particle radiation and LET spectrum so as to carry out a study on the lunar space environment, as well as to reveal the physical process and characteristics of the interaction between the solar wind and lunar soil, and to understand the high-energy particle radiation environment on the Moon surface and its relation to solar activity by measuring fast neutron energy spectra and thermal neutrons flux on the Moon surface.

2.2 Chang'E-4 Payloads and Their Tasks

Totally there are 9 payloads mounted on the Chang'E-4 probe, as shown in Table 1.

3 Latest Scientific Results of Chang'E-4

3.1 Topographic and Geological Characteristics of the Chang'E-4 Landing Area

Liu *et al.*^[8] reconstructed the powered descent trajectory of Chang'E-4 using photogrammetrically processed images of the Chang'E-4 landing camera, navigation camera, and terrain data acquired by Chang'E-2. The study confirmed that the precise location of the Chang'E-4 landing site is 177.5991°E , 45.4446°S with an elevation of -5935 m. The landing site was accurately identified with lunar imagery and terrain data with spatial resolutions of 7 m, 5 m, 1 m, 10 cm and 5 cm per pixel. As shown in Figure 1.

Fu *et al.*^[9] proposed that both of the lander and the rover locate on the basalt impact sputtering in the Von Kármán crater by the analysis results of multi-source high-resolution remote sensing and hyperspectral image data. Li *et al.*^[3] proposed that the geologic setting of the landing site is a region of impact craters superposed on the floor of the SPA basin (the 225-km-diameter Von Kármán crater and the 245-km-diameter Leibnitz crater). Chang'E-4 landing site is about 138 km away from the center of Finsen crater.

Di *et al.*^[5] proposed that the terrain of the landing area is high in the northeast and low in the southwest, and there are undulating waves from the

Table 1 Chang’E-4 payloads and their tasks

Scientific objectives	Tasks	Scientific payloads		
		Lander	Rover	Relay
Low-frequency radio astronomical study on the lunar surface	Characterize low-frequency radio emissions from the Sun, the Solar system and the Milky Way galaxy	Low-frequency Radio Spectrometer		Netherlands-China Low-frequency Explorer
Exploring morphology and mineral constituents of patrol area in Moon’s far side	Acquire optical images related to topography and geomorphology of the landing and roving sites; Acquire infrared images of the landing site	Landing Camera Terrain Camera	Panoramic Camera Infrared Imaging Spectrometer	
Probing shallow structures of patrol area on Moon’s far side	Acquire data related to Lunar soil and sub-surface structure of the lunar crust		Lunar Penetrating Radar	
Study on lunar space environments such as neutrons radiation dose and neutral atoms	Measure neutrons and dose rate on the lunar surface, including the energy spectrum, the flux of these particles, and Linear Energy Transfer (LET); Measure energetic neutral atoms and positive ions on the lunar surface, including the energy, mass and flux of these particles	Lunar Lander Neutrons and Dosimetry	Advanced Small Analyzer for Neutrals	

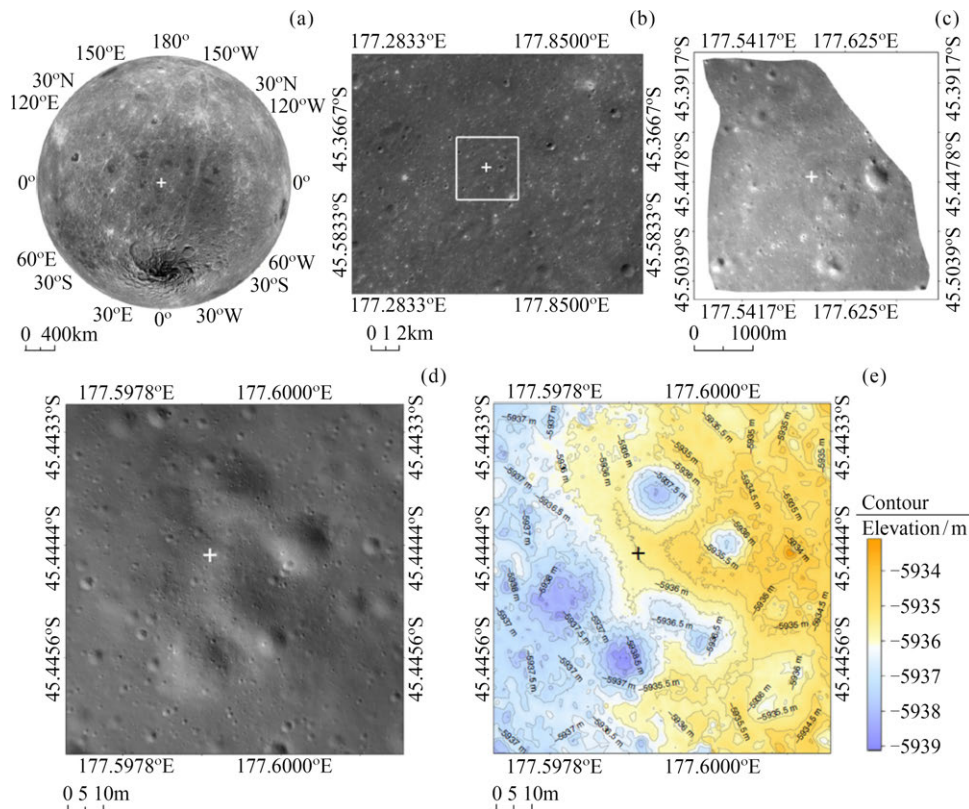


Fig. 1 Location of the Chang’E-4 landing site. The “+” is the identified landing location. (a) (b) Chang’E-2 DOMs, using the Chang’E-4 landing site as the projection center of the azimuth projection. (c) LCAM DOM with a resolution of 5 m per pixel. (d) LCAM DOM generated by the LCAM images with resolutions from 21.4 cm to 0.2 cm per pixel and is uniformly resampled at 5 cm per pixel during mapping. (e) shaded-relief map with a contour line produced by the LCAM DEM, which area and resolution are the same as that in (d)

southeast to northwest. Qiao *et al.*^[10] proposed that the overall terrain around the landing site presents relatively flat, of which the slope of more than 90% of the area is less than 5° (30 m baseline), and few rocks on the Moon surface are exposed. The main geomorphological characteristics of the landing area are represented as a large number of circular craters with a diameter of less than 1 km and secondary craters with cluster-shape or chain-shape, as well generally there are no rocks are exposed near these craters. Other nearby craters are likely to deliver SPA-basin-subfloor material to the landing site. The youngest of these is the 72-km-diameter crater Finsen, which is located to the northeast of the landing site crater. The results are shown in Figure 2^[3]. The Finsen crater is considered to be formed when small bodies impact the surface within the SPA basin. The deep-seated materials below the surface of the SPA basin are excavated, whose ejecta scattered on the plain of the Von Kármán crater^[9].

Di *et al.*^[5] proposed that the ejecta covered over the landing area are 60~70 m thick, at least comprised of two sets of ejecta with approximately perpendicular directions. They further interpreted the superimposition of NE-SW ejecta from Finsen crater

on the underlying SE-NW dome-like surface relief from Alder crater. Numerical simulations predict about 30 and 35 m ejecta deposited at the landing site from Finsen and Alder craters, respectively. Numerical simulations show that the thicknesses of the sputters from Finsen and Alder pits at the landing points are about 30 m and 35 m (Figure 3), respectively.

The study of Fu *et al.* indicated that the boundary between Finsen ejecta and underlying mare basalt at the Chang'E-4 landing site is constrained to a depth of 18 m, shown as in Figure 4. Furthermore, Based on the derived permittivity, Lai *et al.*^[16] gave an estimate for the thickness of fine-grained lunar regolith at the Chang'E-4 location of 11.1 ± 0.4 m.

3.2 Constitution of Deep-seated

Materials of the Moon

The Visible and Near-Infrared Imaging Spectrometer (VNIS) on board the Chang'E-4 rover enabled the first in situ reflectance measurements of the far side of the Moon. The route of the rover experienced 14 lunar days as of January 2020, as shown in Figure 5.

The geological characteristics of the Chang'E-4 landing site indicated that the surface materials

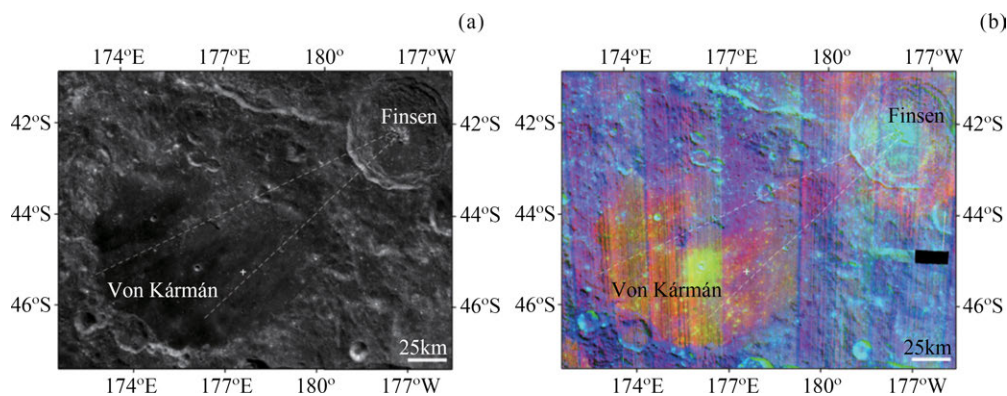


Fig. 2 Distribution of Finsen ejecta in the Von Kármán crater. (a) Chang'E-1 Digital Orthophoto Map; spatial resolution, 120 m. (b) M3 color composite. R, 2- μ m-band center; G, 2- μ m-band depth; B, reflectance at 1580 nm. White dashed lines represent two major northeast-southwest ejecta rays of the Finsen crater converging towards its central peak. The white cross is the Chang'E-4 landing site, which is located on the ejecta material of the Finsen crater. The 2- μ m-band center can be used to distinguish between LCP and HCP. As the content of Fe and Ca in the pyroxene increases, the 2- μ m-band center shifts towards longer wavelengths (redder). The 2- μ m-band depth indicates the relative amounts of mafic minerals. The 1580 nm reflectance represents the brightness of the lunar soils (which can be affected by plagioclase content).

LCP-bearing materials appear light blue, and HCP-bearing materials appear green

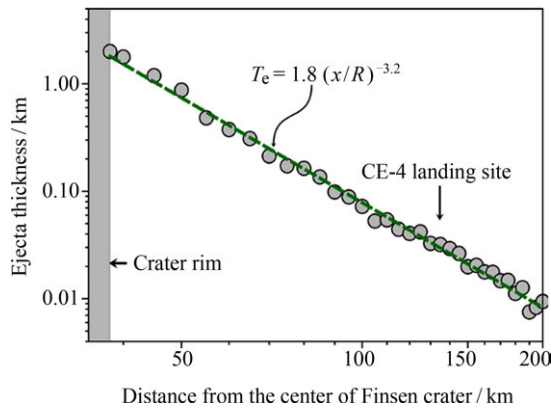


Fig. 3 Ejecta thickness simulation for Finsen crater.

The thickness of ejecta at the Chang'E-4 landing site from Finsen crater is about 32 m. A similar simulation was also carried out for ejecta from Alder crater with a result of about 35 m

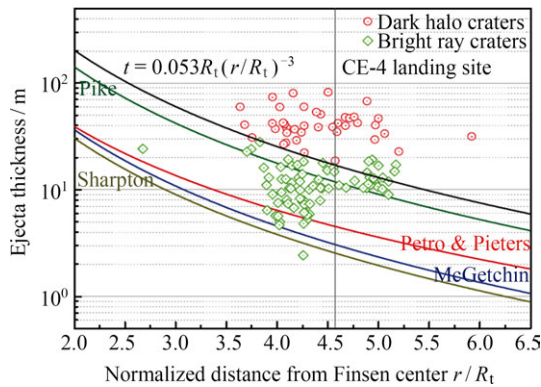


Fig. 4 Thickness estimates for the Finsen ejecta plotted as a function of the distance from Finsen center. The red circles and green diamonds represent the DHCs and BRCs identified in the study area. Their distance from Finsen crater center have been normalized to the transient radius of Finsen crater ($R_t=30.66$ km). The solid curves present the thickness of Finsen ejecta calculated using the different models. The vertical gray line represents the Chang'E-4 landing site ($r=140.15$ km, $r/R_t=4.57$)

explored by the lunar rover were delivered mostly from Finsen^[3,5,9-15]. Li *et al.*^[3] provided the evidence that the deep-seated materials mainly exist as olivine and low calcium pyroxene within the SPA basin, which are the mantle material that exposed the lunar surface. The study of Gou *et al.*^[11] and Yan *et al.*^[14] drew a similar conclusion. However, Hu *et al.*^[15] proposed that the materials may originate from the

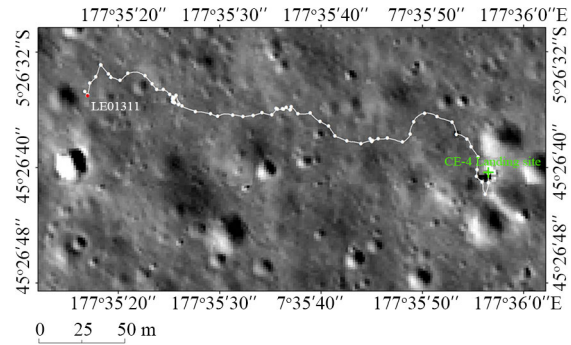


Fig. 5 Route of the Yutu-2 rover drove (as of the 14th lunar days)

ejecta of neighboring crater.

Li *et al.*^[3] studied the radiance spectra of two sites (point S1: CE4_0016 and point A: CE4_0015) adjacent to the lander were collected during the first lunar day, shown in Figure 6. By analysis of VNIS spectra, as shown in Figure 7. the research team find that the absorption characteristics of spectra of soil within the Chang'E-4 landing area are obviously different from those of spectra of mare soil in Mare Imbrium where Chang'E-3 landed in and it presents apparent spectral features of Low-Calcium Pyroxene (LCP) and olivine. The analysis suggests that the materials at the Chang'E-4 landing site exhibit an LCP signature with the existence of rich olivine.

Their results imply that the Chang'E-4 landing site is characterized by mafic components that are dominated by LCP and olivine, with a very small amount of High-Calcium Pyroxene (HCP), suggesting the presence of deep-seated material from the upper mantle. Alternatively, these mafic components might originate from the base of a differentiated melt sheet. Several studies indicate that the impact event that formed the SPA basin might not have excavated through the lunar crust and exposed the mantle material on the surface of the Moon. The study interprets to present the presence of LCP and olivine may originate from the lunar mantle.

Di *et al.*^[5] conducted an analysis using the in-situ spectra of the eleven sites and a rock within the Chang'E-4 landing area. Their study reveals that the surface materials are lunar deep interior material excavated from Finsen crater with possible contributions from Alder crater rather than the underlying

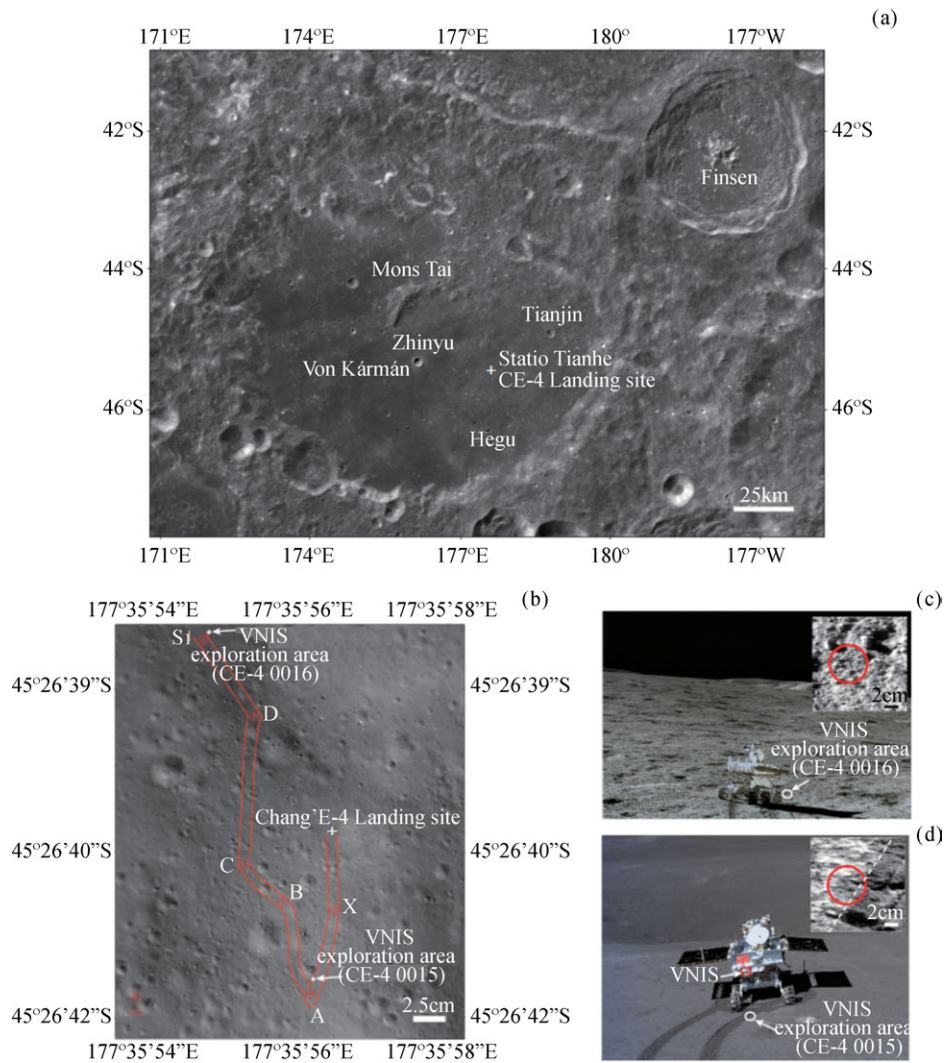


Fig.6 Locations of the Chang'E-4 landing site and the VNIS measurements. (a) The Chang'E-4 landing site on a 7-m-resolution Chang'E-2 Digital Orthophoto map. (b) Yutu-2 rover traverse map and location of VNIS detection points S1 (CE4_0016) and A (CE4_0015) during the first lunar day; red lines are Yutu-2 wheel tracks. (c)(d) Images of the VNIS conducting spectral detection at points of the VNIS conducting spectral detection at points S1 and A on the lunar surface. The images were acquired by the Terrain Camera 5. Insets, 600-nm-band images of points S1 and A, obtained by the VNIS. The red circles show the field view of the SWIR detector, and the white dashed line is the boundary between the rover wheel track and the lunar surface

mare basalt. The constituents of the lunar regolith in the Chang'E-4 landing area are relatively uniform, mainly consist of pyroxene, feldspar and agglutinates, and a small amount of olivine. The ratio of olivine/pyroxene is relatively high. Pyroxene is mainly LCP enriched in magnesium. Their results are shown in Figure 8 and 9^[11, 12]. The composition is likely representative of the materials of the SPA basin floor excavated by the Finsen crater^[5, 11, 12]. Gou *et al.*^[11]

proposed that although it cannot be ruled out that it originated from impacting molten foreign bodies, the regolith and rock fragments observed by the probe are likely to be lunar mantle material excavated in the neighboring Finsen crater.

Lin *et al.*^[12] conducted an in-situ spectrum analysis of a rock with size larger than 20 cm along the driving route of the rover. The results as shown in Figure 10, indicate that the spectrum of the rock is

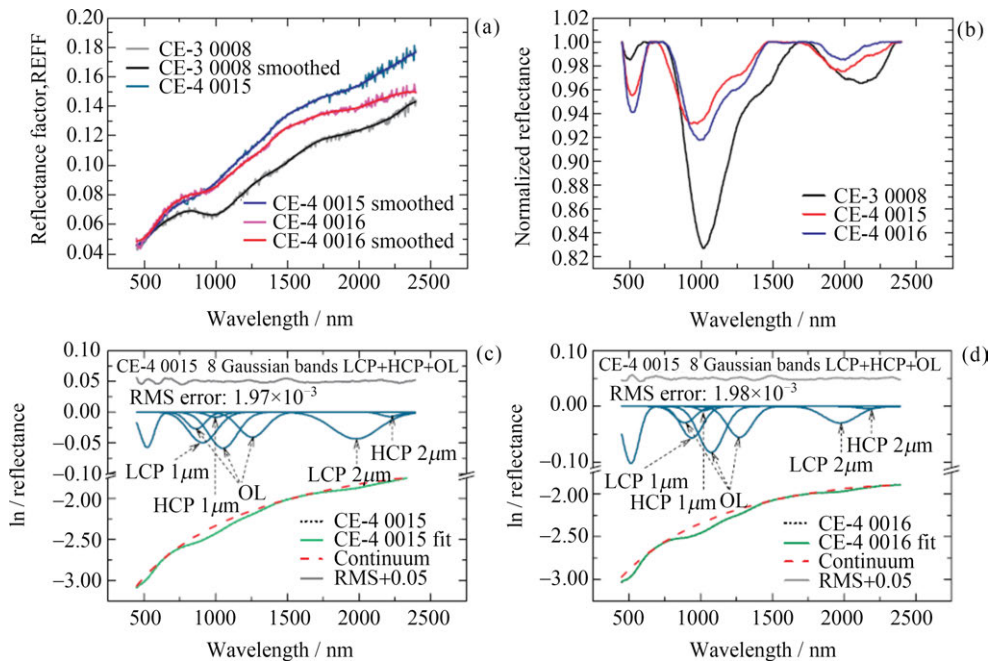


Fig. 7 Chang'E-4 reflectance spectra acquired by the VNIS during the first lunar day. (a) Reflectance (REFF) spectra obtained by Chang'E-4 VNIS (CE4_0015 and CE_0016) and the Chang'E-3 VNIS detection point (CE3_0008). (b) Continuum-normalized spectra of (a). (c) (d) MGM-fitting results for CE4_0015 and CE4_0016 using endmember LCP, HCP and olivine

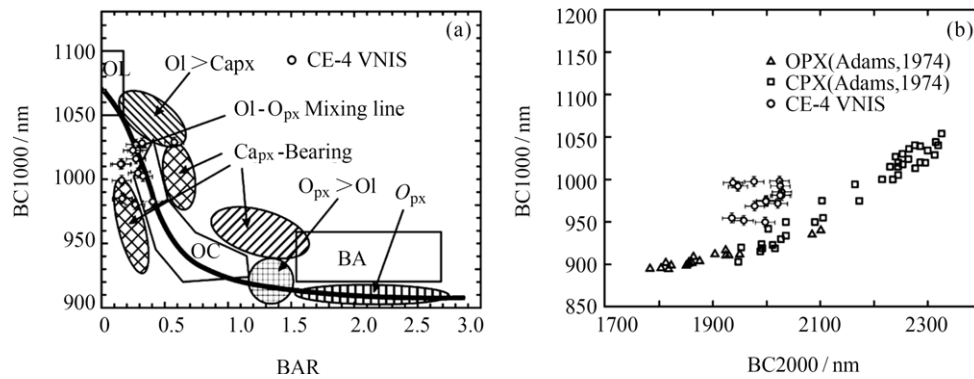


Fig. 8 Scatter plots of spectral parameters. (a) BAR–BC1000; (b) BC2000–BC1000. Reference compositional groups are from Cloutis *et al.* (1986) and Adams (1974), respectively. The error bars in each plot represent a first-order approximation for the uncertainty determined by the law of propagation of uncertainty. Here OC represents ordinary chondrites and BA represents pyroxene dominated basaltic achondrites

similar with that of the lunar regolith and both of them may be the homologous substances. The composition of the rock consists of 38.1%±5.4% low-Ca pyroxene, 13.9%±5.1% olivine and 48.0%±3.1% plagioclase, referred to as olivine-norite. According to the analysis, it is inferred that the rock may be crystallized from the impact-derived melt pool formed

by the SPA impact event *via* mixing the lunar crust and mantle materials, the related results are indicated in Figure 10.

Mare basalts at the landing site are dominated by low-titanium basalts, and appear to be less mafic and iron-depleted than all typical kinds of returned lunar basalt samples and may represent a new kind of

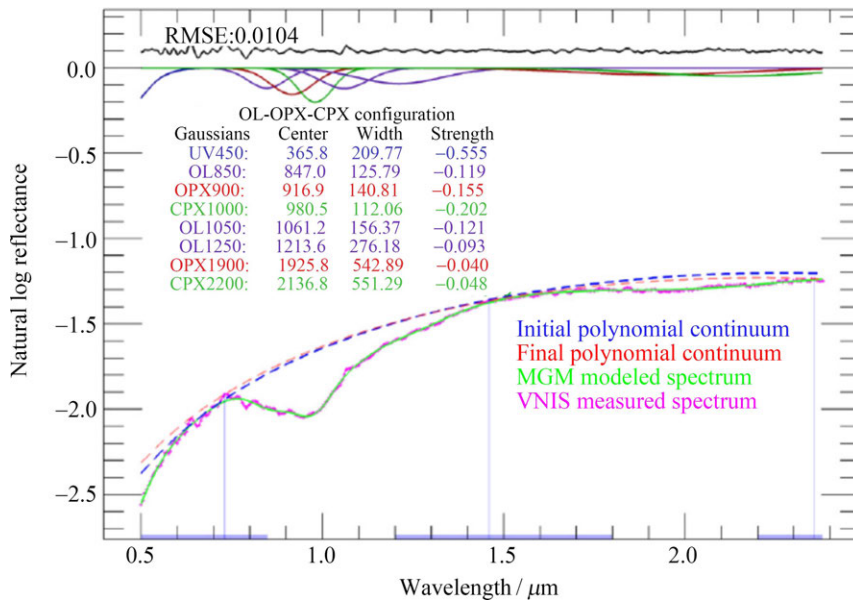


Fig. 9 Rock spectrum modeled with OL-OPX-CPX configuration by MGM

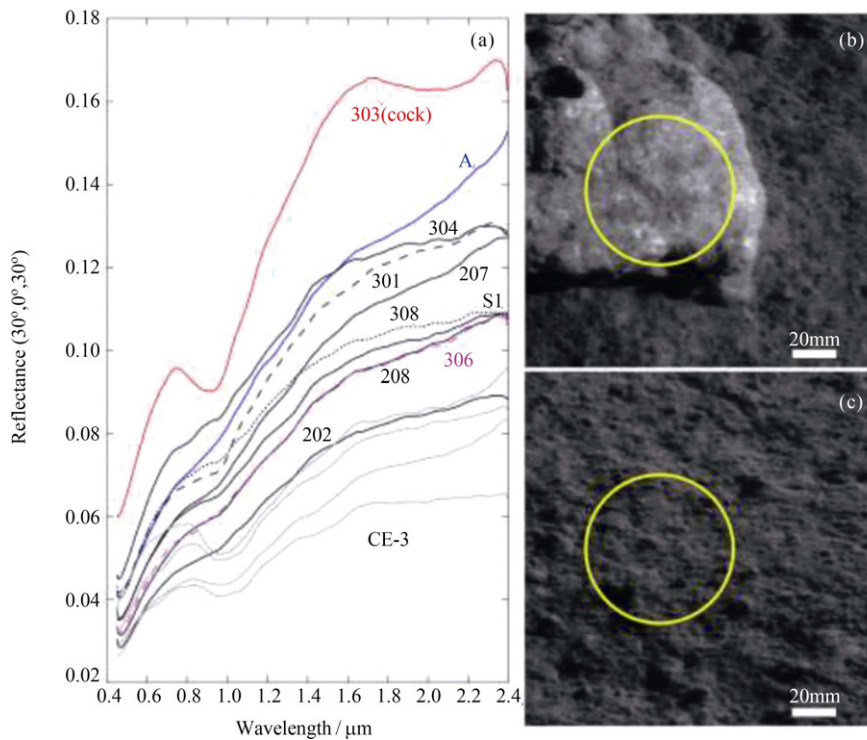


Fig. 10 (a) VNIS spectra of the rock and lunar regolith measured by Chang'E-4. (b) (c) CMOS images of the rock (labeled as 303) and the lunar soil (labeled as 207) at 0.75 μm observed by VNIS imaging spectrometer, respectively. The yellow circle is SWIR field, and the scale bar is 20 mm

mare basalt, as shown in Figure 11 and 12. The landing site mare is heavily sculptured by a set of linear parallel ridged and furrowed textures formed by

ballistic ejecta from the Finsen crater, which is characterized by a more feldspathic composition, while with elevated orthopyroxene abundance, and may

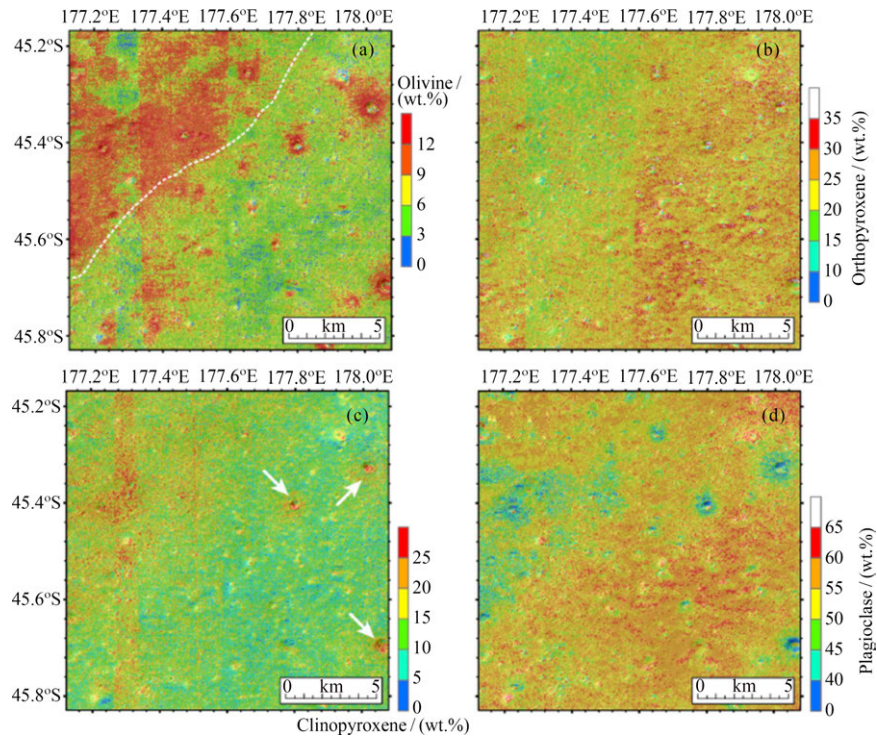


Fig. 11 Major rock-forming minerals of the studied landing area: (a) olivine, (b) orthopyroxene, (c) clinopyroxene, (d) plagioclase, (e) mafic minerals

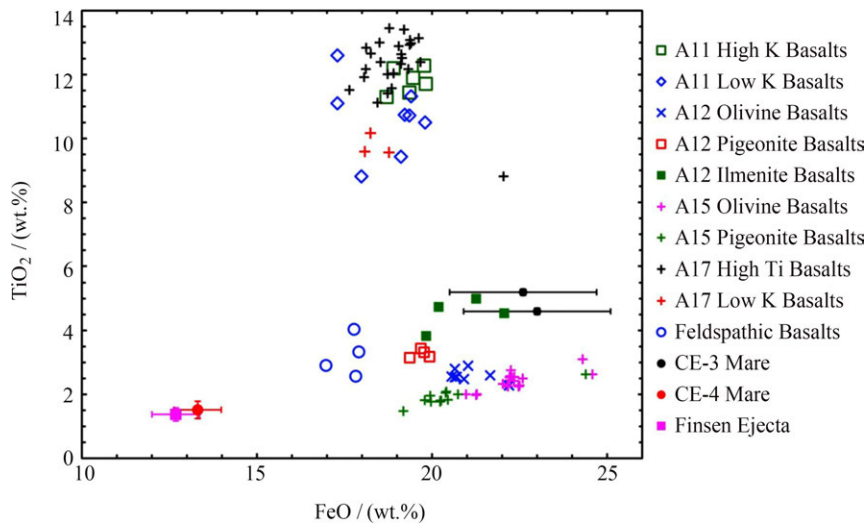


Fig. 12 Comparison of iron and titanium contents for mare basalts and Finsen crater ejecta materials at Chang'E-4 landing site (average values $\pm 1 \sigma$) with all typical kinds of lunar basalts and Chang'E-3 surface in-situ measurements

represent compositional properties of the primitive SPA basin floor materials^[10].

Chisenga *et al.*^[14] performed a 3D inversion of the GRAIL gravity data to produce a density model of the Von Kármán Crater. The results reveal that the region is underlain by a mass excess anomaly

beneath the Von Kármán M Crater with a density of about $3200 \text{ kg}\cdot\text{m}^{-3}$, on the southern rim of the Von Kármán basin. A relatively high-density mass excess anomaly with a density value of up to $3100 \text{ kg}\cdot\text{m}^{-3}$ connects to the first anomaly in the northern part. The study suggests that this was the result of the

buried mare basalts that created a buried impact basin in the Von Kármán M Crater. The occurrence of high-density materials that extend to the lower crust correlates with excavated mantle materials observed on the floor of the Von Kármán basin, suggesting that the impact cratering could have brought upper mantle materials to the surface. The study infers that the evolution of the Von Kármán basin was due to multiple episodes of impact cratering that resulted in crustal reworking and secondary excavation of mantle materials.

Hu *et al.*^[15] conducted an analysis of the main constituents of a large area covering the Finsen crater. Their study proposed that the results indicate a strong correlation between the materials at the landing site and the Finsen crater, and the relevant results are shown in Figure 13. The ejecta of Finsen crater is the major contributor to the surficial materials at the Chang'E-4 landing site. They proposed that the high plagioclase abundance at the landing site may indicate the associated olivine is inherent of anorthosites, rather than the Mg-suite troctolites erupted from the interior of the Moon. The expected

mantle materials are not observed at the Chang'E-4 landing site, indicating that the materials of the present-day crust (at least the upper crust) at the landing area is not the breccia deposits derived from the ejecta of the SPA basin. The relevant results are shown in Figure 13.

3.3 Mineral Abundance and Soil Maturity of the Lunar Surface

Li *et al.*^[3] used four different groups of mineral combinations in the Modified Gaussian Model (MGM) deconvolution: (i) LCP, HCP and olivine (OL); (ii) LCP, HCP and plagioclase (Plag); (iii) LCP and Plag; (iv) LCP and OL. Further analysis on the deconvolved 1- μm -band depth of LCP, HCP and OL suggests that for CE4_0015 the abundances for LCP:HCP:OL are 42%:10%:48%, with the highest abundance for OL, followed by LCP and the lowest abundance for HCP. MGM deconvolution of CE4_0016 (Figure 2d) indicates that LCP:HCP:OL 38%:7%:55%. CE4_0016 is dominated by LCP and OL and has a greater abundance of OL than CE4_0015 and a very small amount of HCP.

Hu *et al.*^[15] utilized a synthesized lunar spectral

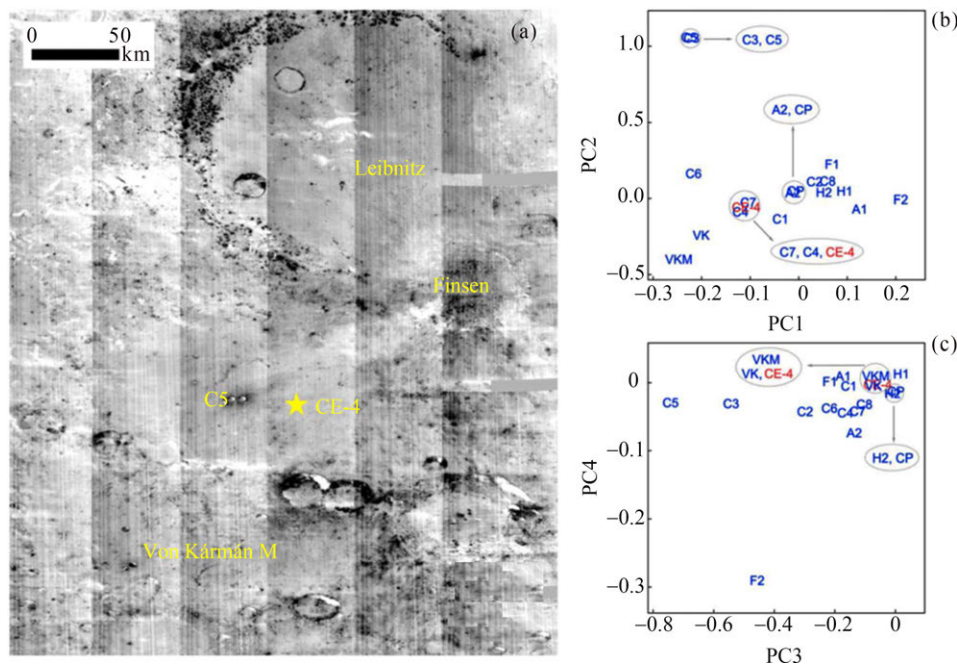


Fig. 13 Principal component analysis results of Chang'E-4 landing site. (a) The image of the fourth principal component (PC4) of the M3 data. (b) PC2 vs. PC1 and (c) PC4 vs. PC3 are distributions of the typical PC values of selected regions of interest calculated from the M3 spectra in the PC space

mineral Lookup Table (LUT) based on radiative transfer models, considered spectra of olivine (OLV), clinopyroxene (CPX), orthopyroxene (OPX), and plagioclase (PLG). The results indicate that the landing site is dominated by PLG (56%~72%), followed by OPX (9%~28%), CPX (4%~19%), and OLV (2%~12%), in relative abundance, in agreement with the results from Kaguya Multiband Imager mineral mapping. The mineral abundances with uncertainties, obtained by averaging the four results, are summarized in Figure 14 and Table 2.

Qiao *et al.*^[10] studied a detailed geologic context,

topographical, morphological, geochemical and mineralogical characterization of a 20 km×20 km area centered at the Chang'E-4 landing area. The result indicated that the majority (> 80%) of the landing area has calculated FeO content between 11% and 13%wt. and > 95% of the regional surface has TiO₂ content between 1% and 2%wt. The result is shown in Figure 15. The studied landing area surface was divided into two major units with slightly different iron contents: a northern belt region with relatively elevated FeO abundance (about 13%~14% wt., the mean value of 13.3%wt. with $1\sigma = 0.7$) and a broader

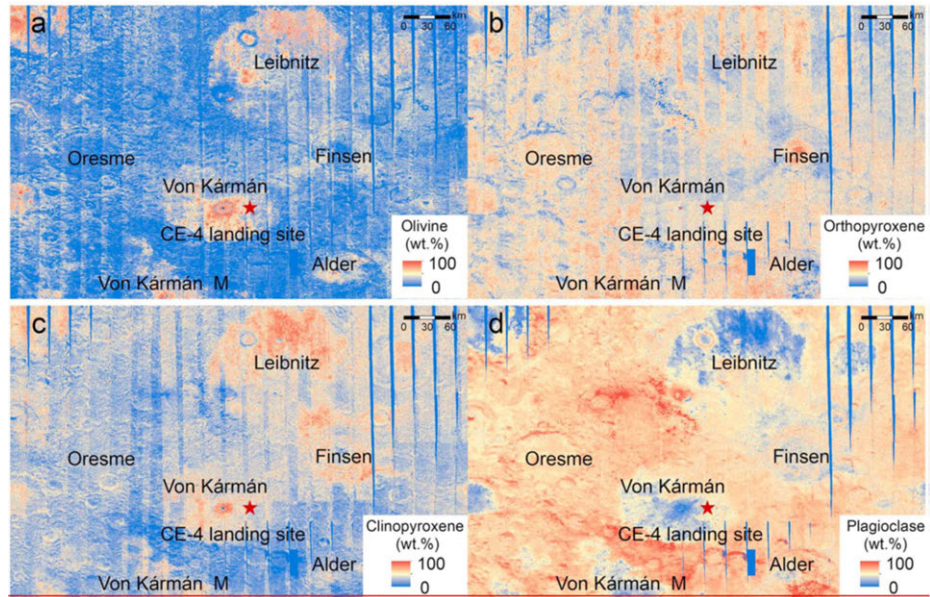


Fig. 14 Mineral mapping results. (a) Olivine mineral abundance, (b) orthopyroxene mineral abundance, (c) clinopyroxene mineral abundance, and (d) plagioclase mineral abundance

Table 2 Mineral abundance (%wt.) obtained by comparing the CE-4 data and the LUT spectra, and the errors were obtained by using equation (S8)

Data	First lunar day		Second lunar day				Average
	N15	N16	N17-1	N17-2	N18-1	N18-2	
OLV	9.0±1.0	11.1±3.9	2.1±2.1	7.9±2.3	11.8±2.2	10.9±2.5	8.8±3.3
OPX	27.5±3.4	9.2±4.5	24.0±0.6	17.8±1.1	20.3±2.5	10.9±2.5	18.3±6.6
CPX	4.1±0.3	8.5±0.3	14.0±1.7	18.8±0.7	10.6±3.1	6.8±1.2	10.4±4.8
PLG	59.5±2.6	71.3±8.1	60.0±1.0	55.5±2.7	57.3±1.6	71.5±3.8	62.5±6.4
$i/(\circ)$	50.88	72.06	73.39	64.51	64.56	66.23	—
$e/(\circ)$	46.93	42.89	47.97	46.53	46.30	45.48	—
$a/(\circ)$	93.97	89.55	77.81	91.87	90.82	101.93	—

Note i , e , and α are solar zenith angle, sensor viewing zenith angle, and the solar phase angle, respectively. LUT=lookup table; OLV=olivine; OPX=orthopyroxene; CPX=clinopyroxene; PLG=plagioclase.

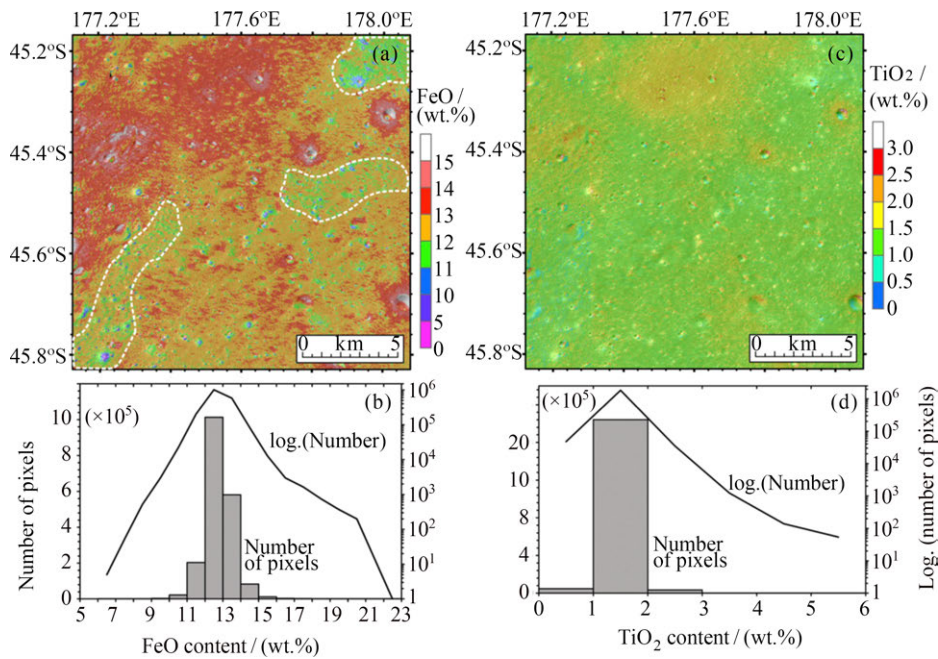


Fig. 15 FeO (a) and TiO₂ (c) abundance maps of the studied landing area and their histograms (b) (d).

The dashed patches in (a) mark the strip-shaped areas with decreased iron contents

region with slightly lower FeO abundance (about 12%~13%wt., the mean value of 12.7%wt. with $1\delta=0.7$).

Ling *et al.*^[13] presented a comprehensive study of the composition, mineralogy, and chronology of the basaltic and non-mare units in this crater, with the intent to provide context for the compositional properties of the landing site. They produce the compositional maps such as FeO, TiO₂, Mg[#] and Th, and analyze spatial distribution characteristics of monoclinic pyroxene and orthopyroxene. The mare surface in Von Kármán crater is relatively low in FeO (about 13%~18%wt.) and TiO₂ (about 1%~3%wt.) in comparison with basalt at the Chang'E-3 landing site (*i.e.*, about 22.8%wt. FeO and 5.0%wt. TiO₂). It is clear that the typical mare basalt belongs to a low-Fe (15.3%±0.6%wt.) and low-Ti (2.0_0.3%wt.) end-member, while the Mg composition suggests they are relatively high in Mg[#] values (about 52±2). The related results are shown in Figure 16. Chang'E-4 mare basalt stands out as a special type of basalt with similar Fe, Ti contents, and Mg[#] values with the very high K basalt and high aluminum basalt from Apollo 14 (*e.g.*, Apollo 14053, 14168, 14305, 14321 samples) and Luna 16 missions^[10,13]. The characteri-

stic chemical compositions of Chang'E-4 basalt may imply a unique view of farside volcanism^[13].

3.4 Geological Evolution of the Von Kármán Crater

Ling *et al.*^[9,13] used the remote sensing data to identify two types of impact craters, which are indicated by 40 dark rings and 77 bright rings in the landing area. The dark ring impact crater can be regarded as the ejecta from Finsen crater, which can penetrate the surface layer of the landing area and excavate the lower basalt, whileas impact craters indicated by the bright ring are not able to penetrate the ejecta layer. The research teams produced the schematic of stratigraphy and subsurface structure of the Chang'E-4 landing site and analyze the coverage relationship of ejecta over multiple times in this area, as shown in Figure 17. The study reveals the stratigraphic structural characteristics and geological evolution history of the landing area. The related results are shown in Figure 17 and 18.

A brief geological history of the study area is proposed as follows.

(1) The South Pole-Aitken basin was formed more than four billion years ago^[13,14] in the multiple cratering scenario created the SPA that eventually

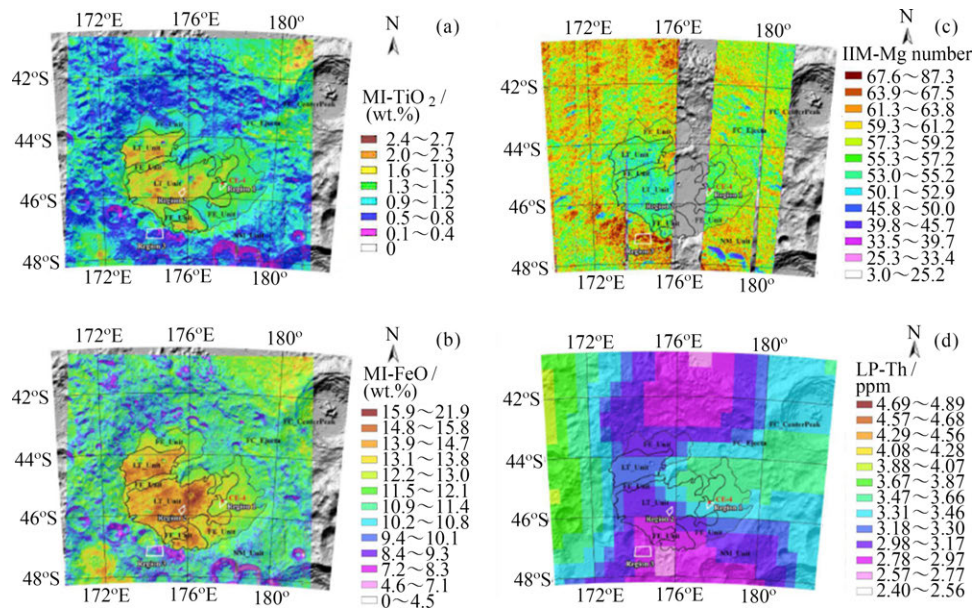


Fig. 16 Chemical compositions of Von Kármán crater. (a) TiO_2 map and (b) FeO map using Kaguya Multiband Imager (MI) data, (c) $Mg^\#$ ($100 \times MgO / (MgO + FeO)$) map using Chang'E-1 IIM data, and (d) Th maps from Lunar Prospector data. The base map is LOLA shaded relief image. Black polygons are the unit division results: LT, low-titanium mare unit; FE, Finsen ejecta unit

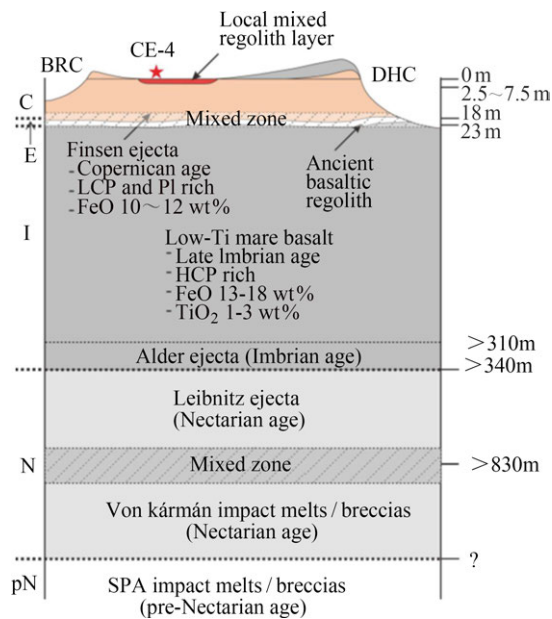


Fig. 17 Stratigraphy and subsurface structure. The red star indicates the Chang'E-4 landing site. Typical DHCs and BRCs are shown here.

The shaded regions indicate the mixed zone between the impact ejecta and the underlying layer. The letters on the left represent lunar geological periods: pN for pre-Nectarian, N for Nectarian, I for Imbrian, E for Eratosthenian, and C for Copernican

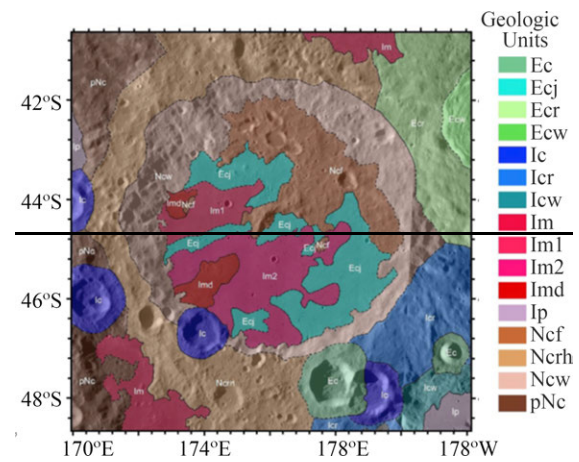


Fig. 18 Geologic map of Von Kármán crater. pNc is pre-Nectarian crater materials, Ncw, Ncrh, Ncf are Nectarian crater wall, hummocky rim, and floor materials, Ip is Imbrian plain materials, Im, Im1 and Im2 are Imbrian mare units, Imd is Imbriaum dome-like unit, Ic is Imbrian materials and can be sub-divided into rim (Icr) and wall (Icw) units, Ec is Eratoshenian crater materials and can be sub-divided into rim (Ecr), wall (Ecw) and ejecta (Ecj) units excavated the lower crust and probably the upper mantle, resulting in a very thin crust region^[14].

(2) A Nectarian impact event formed 186-km-

diameter Von Kármán; Then, the 240-km-diameter Leibnitz crater formed north of Von Kármán crater and destroyed part of the northern rim structure of Von Kármán crater and ejected material into the northern part of the Von Kármán crater floor^[9,13]. The formation of Alder crater also transported a thin layer of exhumed materials^[9].

(3) During the Imbrian period, regional lava-infilling events took place within the SPA basin interior, which generated small mare plains. The Von Kármán floor surface mare deposits are dated to be about 3.4~3.6 Ga, with buried mare flows to be about 3.7 Ga lava flow at a depth of >100 m^[13]. Basaltic volcanism was active at 3.6 Ga, and low-Ti basalt flows filled most of the floor; A basaltic regolith layer formed on the surface of the mare basalt plain^[9]. Mare basalts emplaced at the Von Kármán crater floor are characterized by a Ca- and Fe-rich pyroxene composition, with relatively low iron and titanium contents, but relatively higher magnesium^[13].

(4) In the long Eratosthenian Period, no large crater formed in the adjacent area, and basaltic regolith formed on the surface of mare basalt; The Copernican Finsen impact ejecta overlay the basalt unit and covered the study area; The following small impact events struck the surface, and some of them excavated the underlying basaltic materials and formed the craters with dark halos. These Finsen ejecta materials are characterized by elevated FeO, TiO₂,

and LCP content than typical lunar highlands^[13].

3.5 Stratigraphy Structure of the Lunar Regolith

Lai *et al.*^[16] interpreted the lunar penetrating radar detection data. Indicated at the Chang'E-4 site, the permittivity is about 4.3 at 130 ns, the instantaneous permittivity increases very rapidly at the near-surface section of the regolith (< 2 m) and then grows slowly to the maximum value of about 4.5 at the depth of 11 m. The study derives a bulk density for the regolith at Chang'E-4 of $\rho=1.22\sim 2.23\text{ g}\cdot\text{cm}^{-3}$, increasing with depth.

Radargrams of both LPR experiments show a complicated picture of the shallow stratigraphic profile (Figure 19): numerous short lateral reflectors caused by the accumulation of ejecta from small local craters appear in the near-surface region. Several rough and intermittent interfaces (hr1~3) with rocks and paleoregolith admixed are identified in the Chang'E-4 LPR results, which may correspond to more than one large-scale ejecta layers (hr1) or the transition zones between regolith and bedrock (hr2, hr3). The rough interface above the fractured bedrock at the depth of 25.8 m (hr4) and 33~35 m (hr5) are also revealed by the LPR. Hr3 might be caused by a rough interface of fractured bedrock and hr4 may indicate the rough interface of another fractured paleo basalt layer^[16].

Li *et al.*^[17] combined the information provided by the radargram, the tomographic image, and the quantitative analysis, concluded that the subsurface

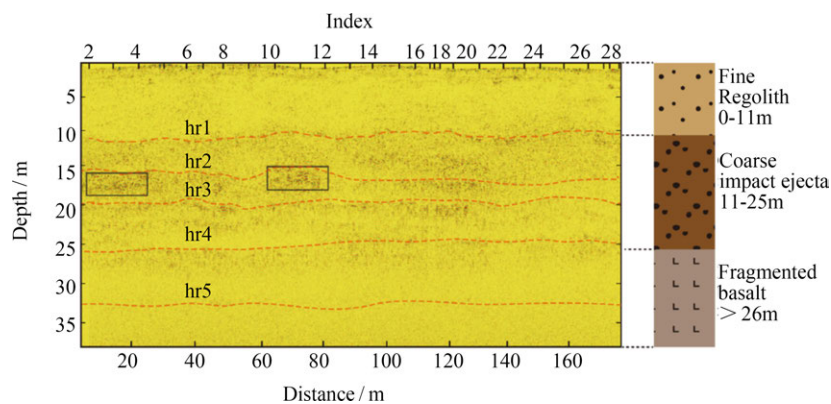


Fig. 19 LPR radargram of CE-4 site. The geologic interpretation of LPR results is given on the panel on the right. hr stands for the horizontal reflector, also indicated by the dotted line. The rectangles circled the hyperbolic signals caused by the discrete scatters within the ejecta layers

internal structure at the landing site is essentially made by low-loss, highly porous granular materials embedding boulders of different sizes. Given such a strong geological constraint, the most plausible interpretation is that the sequence is made of a layer of regolith overlaying a sequence of ejecta deposits from various craters (Figure 20), which progressively accumulated after the emplacement of the mare basalts on the floor of Von Karman crater. The layer of regolith (Unit 1) is quite thick (up to 12 m), is rather homogenous both laterally and vertically, and is mostly composed of fine materials. It developed from the uppermost portion of the ejecta deposits, which were thicker than 12 m and were delivered to this area by multiple impact craters, mostly Finsen, Von Karman L, and Von Karman L' craters. Unit 2 (depth, 12 to 24 m) is characterized by large rocks and boulders that are interbedded with thin layers of fine materials. It is likely formed due to a combination of (i) coarse ejecta that were not mobilized during the landing of impact ejecta, (ii) structural disturbances in local materials caused by the landing ejecta, and (iii) fine materials generated during or after the ejecta deposition. Unit 3 (24 to 40 m)

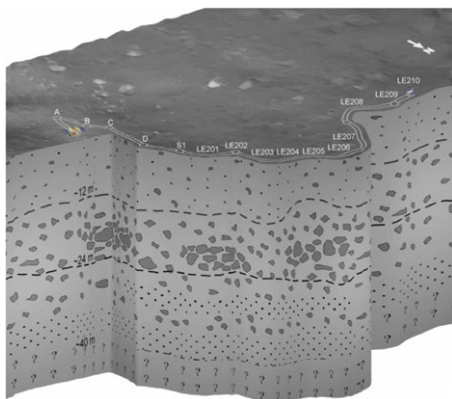


Fig. 20 Schematic representation of the subsurface geological structure at the Chang'E-4 landing site inferred from LPR observations. The subsurface can be divided into three units: Unit 1 (up to 12 m) consists of lunar regolith, Unit 2 (depth range, 12 to 24 m) consists of coarser materials with embedded rocks, and Unit 3 (depth range, 24 to 40 m) contains alternating layers of coarse and fine materials

contains alternating layers of coarse and fine materials. This unit can be interpreted as a combination of ejecta deposits, which were delivered by various craters older than Finsen and regolith developed during the impact intervals.

4 Conclusions and Future Scientific Research

The research team of Chang'E-4 achieved preliminary results in some aspects of lunar science such as terrain, geomorphology, geological tectonic, mineral constitution and shallow subsurface structure by use of data acquired from Chang'E-4. The results of the radar data collected by the LPR provide the first electromagnetic image of the farside subsurface structure and the first "ground truth" of the stratigraphic architecture of an ejecta deposit. The results could provide strong evidence for the understanding of materials in the lunar interior as well as provide new constraints for revealing the important scientific issues, of which the geological evolution of the SPA basin of the Moon, the early evolutionary history of the lunar crust, the structure in the lunar interior and its formation mechanism.

The study on the lunar-based low-frequency radio astronomy, lunar neutron radiation and neutral atoms are still undergoing, with related papers under review. It is believed that more new scientific results are coming up next.

The rover of Chang'E-4 mission works very well on the Moon's far side. Based on the scientific results achieved in the past time, in situ exploration on the Moon's farside by Chang'E-4 is still concentrates on the Finsen crater ejecta and lunar mare basalt around the landing site. However, many scientific issues, such as in the following aspects, still await further investigation.

(1) To cumulate more scientific evidence of whether the deep-seated materials of the Moon's farside originate from the lunar mantle.

(2) To further analyze and interpret scientific data emphatically to study on the mixed-effects of the local basalt and exogenous feldspathic materials.

(3) To conduct further study on the layer structure and geological evolution of the landing area.

(4) To study the transformation of the lunar surface by impacts; volcanic activity scale and their history.

(5) To search clues to the early evolution of the universe, planetary radios of the solar system, and solar low-frequency radio bursts through Low-frequency radio detection.

(6) To study on the relationship between the neutral atom energy spectrum and the solar wind speed, and to measure the electron particle radiation dose, fast neutrons, thermal neutrons and γ -rays on the lunar surface. Discovery in the solar energetic particle acceleration and transport in the heliosphere are expected.

References

- [1] XU Lin, ZOU Yongliao, QIN Lang. Latest Scientific Results of China's Lunar Exploration Program [J]. *Chin. J. Space Sci.*, 2018, **38**(5):598-603
- [2] JIA Yingzhuo, ZOU Yongliao, PING Jinsong. The scientific objectives and payloads of Chang'E-4 mission [J]. *Planet. Space Sci.*, 2018, **162**(SI):207-215
- [3] LI Chunlai, LIU Dawei, LIU Bin, *et al.* Chang'E-4 initial spectroscopic identification of lunar far-side mantle-derived materials [J]. *Nature*, 2019, **569**:378-393
- [4] SPUDIS P D; REISSE R A; GILLIS J J. Ancient multiring basins on the Moon revealed by Clementine laser altimetry [J]. *Science*, 1994, **266**(5192):1848-1851
- [5] KAICHANG D I, ZHU Menghua, YUE Zongyu, LIN Yangting. Topographic evolution of Von Kármán crater revealed by the lunar rover Yutu-2 [J]. *Geophys. Res. Lett.*, 2019, **46**(22):12764-12770
- [6] WU Weiren, LI Chunlai, WEI Zuo, *et al.* Lunar farside to be explored by Chang'E-4 [J]. *Nat. Geosci.*, 2019, **12**(4):222-223
- [7] HUANG J, XIAO Z, FLAHAUT J, *et al.*, Geological characteristics of Von Kármán Crater, Northwestern South Pole-Aitken Basin: Chang'E-4 landing site region [J]. *J. Geophys. Res.: Planets*, 2018, 123:1684-1700
- [8] LIU Jianjun, REN Xin, YAN Wei, *et al.*, Descent trajectory reconstruction and landing site positioning of Chang'E-4 on the lunar farside [J]. *Nat. Commun.*, 2019. DOI:10.1038/s41467-019-12278-3
- [9] FU Xiaohui, QIAO Le, ZHANG Jiang, *et al.* The subsurface structure and stratigraphy of the Chang'E-4 landing site: orbital evidence from small craters on the Von Kármán crater floor [J]. *Res. Astron. Astrophys.*, 2020, **20**(1):1-14
- [10] QIAO Le, LING Zongtheng, FU Xiaohui. Geological characterization of the Chang'E-4 landing area on the lunar farside [J]. *ICARUS*, 2019, **333**:37-51
- [11] GOU Sheng, DI Kaichang, YUE Zongyu. Lunar deep materials observed by Chang'E-4 rover [J]. *Earth Planet. Sci. Lett.*, 2019, **528**:115829
- [12] LIN Honglei, HE Zhiping, YANG Wei, Lin Yangting. Olivine-norite rock detected by the lunar rover Yutu-2 likely crystallized from the SPA impact melt pool [J]. *Natl. Sci. Rev.*, 2019, 183
- [13] LING Z, QIAO L, LIU C, *et al.* Composition, mineralogy and chronology of mare basalts and non-mare materials in Von Kármán crater: landing site of the Chang'E-4 mission [J]. *Planet. Space Sci.*, 2019, 104741
- [14] CHISENGA Chikondi, YAN Jianguo, ZHAO Jiannan, *et al.* Density structure of the Von Karman crater in the Northwestern South Pole-Aitken basin: initial subsurface interpretation of the Chang'E-4 landing site region [J]. *Sensors*, 2019, **19** (20):4445
- [15] HU Xiaoyi, MA Pei, YANG Yazhou, *et al.* Mineral abundances inferred from in situ reflectance measurements of Chang'E-4 landing site in South Pole-Aitken Basin [J]. *Geophys. Res. Lett.*, 2019, **46** (16):9439-9447
- [16] LAI Jialong, XU Yi, ZHANG Xiaoping, *et al.* Comparison of dielectric properties and structure of lunar regolith at Chang'E-3 and Chang'E-4 landing sites revealed by ground-penetrating radar [J]. *Geophys. Res. Lett.*, 2019, **46**:12783-12793
- [17] LI Chunlai, SU Yan PETTINELLI Elena, *et al.*, The Moon's farside shallow subsurface structure unveiled by Chang'E-4 Lunar Penetrating Radar [J]. *Sci. Adv.*, 2020, **6**:6898